Phonon dispersion and low-energy anomaly in CaC$_6$ from inelastic neutron and x-ray scattering experiments

Matteo d'Astuto,[*] Matteo Calandra, Nedjma Bendiab,[†] Geneviève Loupias, and Francesco Mauri

Institut de Minéralogie et de Physique des Milieux Condensés (IMPMC), Université Pierre et Marie Curie-Paris 6, case 115,
4 place Jussieu, 75252 Paris Cedex 05, France[‡]

Shuyun Zhou

Materials Sciences Division, Lawrence Berkeley National Laboratory, Berkeley, California 94720, USA
and Department of Physics, University of California, Berkeley, California 94720, USA

Jeff Graf

Materials Sciences Division, Lawrence Berkeley National Laboratory, Berkeley, California 94720, USA

Alessandra Lanzara

Materials Sciences Division, Lawrence Berkeley National Laboratory, Berkeley, California 94720, USA
and Department of Physics, University of California, Berkeley, California 94720, USA

Nicolas Emery,[§] Claire Hérold, and P. Lagrange

Institut Jean Lamour - UMR 7198 CNRS - Nancy-Université - UPV-Metz - Département Chimie et Physique des Solides et des Surfaces -
Faculté des Sciences et Techniques, BP 70239 - 54506 Vandoeuvre-lès-Nancy Cedex-France

Daniel Petitgrand

Laboratoire Léon Brillouin, CEA–CNRS, CEA-Saclay, 91191 Gif sur Yvette, France

Moritz Hoesch[∥]

European Synchrotron Radiation Facility, BP 220, F-38043 Grenoble Cedex, France
(Received 15 November 2009; revised manuscript received 15 February 2010; published 18 March 2010)

We report measurements of phonon dispersion in CaC$_6$ using inelastic x-ray and neutron scattering. We find good overall agreement, particularly in the 50 meV energy region, between experimental data and first-principles density-functional-theory calculations. However, on the longitudinal dispersion along the (111) axis of the rhombohedral representation, we find an unexpected anticrossing with an additional longitudinal mode, at about 11 meV. At a comparable energy, we observe also unexpected intensity on the in-plane direction. These results resolve the previous incorrect assignment of a longitudinal phonon mode to a transverse mode in the same energy range. By calculating the electron susceptibility from first principles we show that this longitudinal excitation is unlikely to be due to a plasmon and consequently can probably be due to defects or vacancies present in the sample.

I. INTRODUCTION

Intercalation of foreign atoms in graphite can stabilize superconductivity by introducing metal atoms between the layers, which allow both tuning of the interlayer spacing and charging of the graphite host. For a long time it was believed that the maximum critical temperature obtainable at ambient pressure in graphite intercalation compound (GIC) (Ref. 1) was less than 2 K. The discovery of high-temperature super-conductivity in two intercalated compounds: YbC$_6$ (Ref. 2) and CaC$_6$ (Refs. 2 and 3) with unprecedented high transition temperatures, 6.5 K and 11.5 K respectively, has raised renewed interest about the role of phonons in GICs.

The role of the in-plane and out-of-plane phonon modes in CaC$_6$ has been controversial. By using the density-functional theory (DFT), it has been shown that super-conductivity in CaC$_6$ is due to an electron-phonon mechanism.[4–6] The electron-phonon coupling is mainly associated to carbon vibrations perpendicular to the planes of graphite (C$_z$), and calcium vibrations parallel to the graphite planes (Ca$_{xy}$). However specific-heat measurements suggest[7] that the contribution of C$_z$ vibrations is even larger than what was predicted by DFT. Consequently, it would be desirable to measure the phonon dispersion of CaC$_6$ in order to see if there is actually a disagreement between theory and experimental data.

In this work we measure phonons in CaC$_6$ along the (111) axis of the rhombohedral representation using inelastic x-ray and neutron scattering (IXS and INS, respectively). Furthermore, in order to asses the precision of DFT simulations we compare the calculated and measured in-plane averaged IXS structure factor.

On the longitudinal dispersion along the (111) axis of the rhombohedral representation, we find an unexpected anticrossing with an unidentified additional mode, at about 11 meV. At the same energy, we observe also unexpected intensity on the in-plane direction.
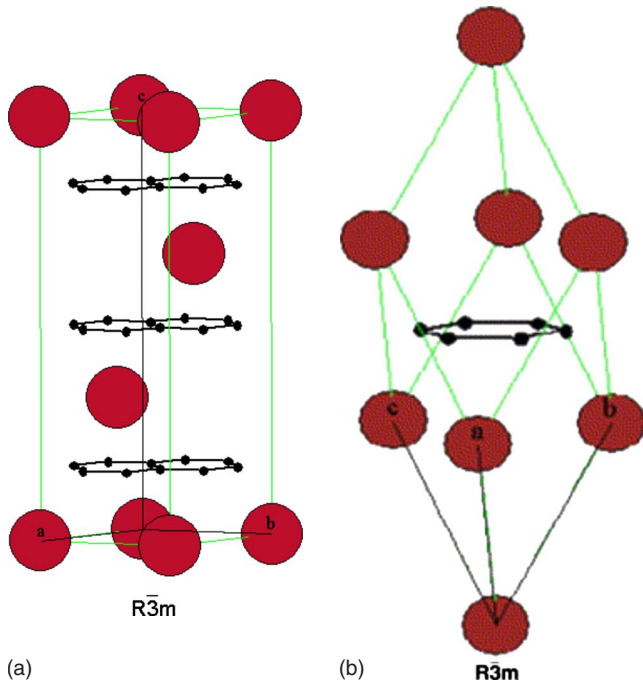
FIG. 1. (Color online) Right panel: rhombohedral crystal structure of CaC_6. Large red circles correspond to calcium ions and small black ones to carbon atoms. Left panel: the corresponding hexagonal unit cell. The three-rhombohedral c axis is perpendicular to the honeycomb graphene planes.

Previous measurements of phonon dispersion in CaC_6 (Ref. 8) assign a longitudinal character to a mode in the same energy range but the mode is transverse. Here we show that and additional mode appear in the same energy region and interact with the longitudinal-acoustic mode. This result could help to resolve this apparently incorrect mode assignment.

II. METHOD

IXS and INS measurements have been conducted on a polycrystalline sample of highly oriented pyrolytic graphite intercalated with Ca, prepared by liquid-solid synthesis method in lithium-based alloys.[9] The sample shows same superconducting properties[10] as previously reported on samples prepared using the same method.[3]

Phonon measurements in graphite are a classical example of comparison between IXS and INS, as shown at the very beginning of the IXS technique by Burkel.[11] The IXS approach is particularly favorable for high energy modes as it is the case in graphite and GICs where some optical branches involving carbon ions are in the 170 meV energy range.[12]

In this kind of sample the polycrystalline domains are actually aligned along a crystal direction, corresponding to the (111) axis in the rhombohedral structure of CaC_6 (Ref. 13) (see Fig. 1). As a consequence, the phonon dispersion of the longitudinal modes, with momentum parallel to the (111) direction, can be measured. The different carbon layers in the sample are randomly rotated respect to the common (111) axis so that the IXS measurement for a given momentum of
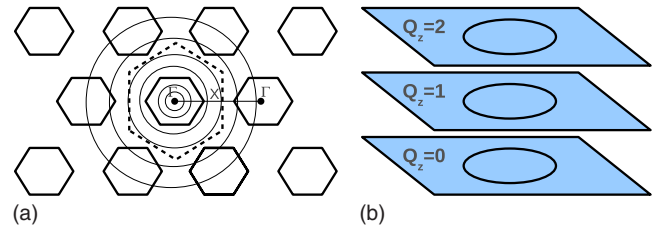

FIG. 2. (Color online) Top panel: section of the rhombohedral reciprocal space corresponding to the a^*b^* plane of the graphite sublattice in CaC_6. Circle corresponds to fixed Q lines in the plane. Two Γ points in different hexagons are shown. The line connecting the two Γ points is parallel to $(1\bar{1}0)$. The large, dashed hexagon indicate the projection of the rhombohedral Brillouin zone, with X the zone boundary along $(1\bar{1}0)$. Bottom panel: the circles can be shifted in different Brillouin zones along the graphite c^*, adding a component $Q_z \times (1\ 1\ 1)$. The L point lies halfway between two planes at $Q_z \times (1\ 1\ 1) + (0.5\ 0.5\ 0.5)$.

modulus Q in the a^*b^* plane will be an average over a circle of radius Q, as shown in Fig. 2, top panel. The volume of the sample we measured was enough for a measurement of the longitudinal phonon dispersion along (1 1 1) using INS, but the signal from the in-plane average was way too weak for neutron, while strong enough for IXS. Therefore we decided to couple the two probes in order to achieve an extensive insight on the phonon structure of CaC_6.

The IXS experiment was carried out on the undulator ID28 beamline at the ESRF. We have chosen to work with the Si (9 9 9) (Refs. 14 and 15) reflection with a wavelength of 0.6968 Å^{-1} (17 794 eV) and an energy resolution $\Delta E = 3.0 \pm 0.2$ meV.[16] Additional spectra were collected using the Si (11 11 11) reflection with a wavelength of 0.5701 Å^{-1} (21 747 eV) and an energy resolution $\Delta E = 1.5 \pm 0.1$ meV. The backscattered beam is focused on the sample position by a gold-coated toroidal mirror, which provides a focal spot of $h \times v = 0.270 \times 0.090$ mm^2 full width at half maximum. Further details of the used configuration are described in Ref. 17. The sample measured in IXS is a platelet with thickness of ~0.25 mm along (1 1 1) direction and an area of 4.2 $\times 0.9$ mm^2. The sample was hold in a Lindemann glass capillary, sealed in a glove box.

The inelastic neutron scattering experiment was carried out on the cold source 4F2 and thermal source 2T triple-axis spectrometer at the Laboratoire Léon Brillouin in Saclay, France. Harmonic contribution from the monochromator was reduced using a standard graphite filter, so final neutron wave number was typically of 1.975 Å^{-1} for 4F2, and of 2.662 or 4.100 Å^{-1} for 2T although some scan at 1.975 Å^{-1} was taken for comparison sake or for averting artifacts from monochromator harmonics. Collimation were of 60'-open-sample-open-open, and with a horizontally focusing monochromator and a vertically focusing analyzer. Several platelets, of about 6 mm width and for a total of 2 mm thickness, were kept together in an aluminum foil. The sample was sealed in an aluminum can, sealed in a glove box, using an indium gasket.

A comparison of the IXS and INS data is shown for a point along the Γ-L line in Fig. 3. In parallel to IXS and INS
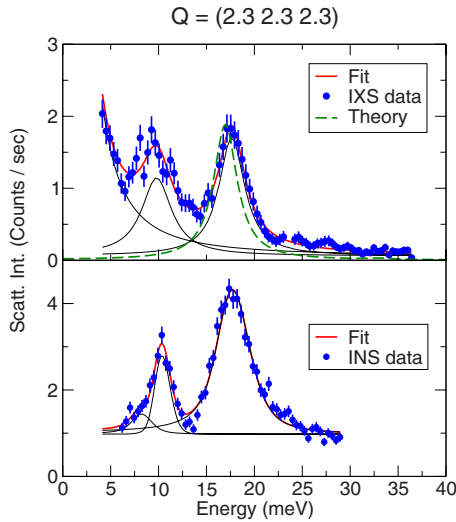
FIG. 3. (Color online) Inelastic x-ray (top panel) and neutron (bottom panel) energy loss spectra at $\mathbf{Q} = \mathbf{G} + \mathbf{q} = 2 \times (1,1,1) + (0.3, 0.3, 0.3)$, corresponding to a longitudinal phonon polarization along 0.6 of the Γ-L line. Data are fitted using a convolution of the instrumental function with an harmonic oscillator. In the top panel, theoretical calculations have been included (dashed lines).

data we carried out first-principles density-functional-theory calculations in the linear response.[18,19] We use the generalized gradient approximation[20] and ultrasoft pseudopotentials.[21] Technical details are the same as in Refs. 4 and 22.

III. EXPERIMENTS AND DISCUSSION

Figure 4, top panel, shows the measured phonon dispersion along the c axis using IXS and INS, as compared with first-principles calculations. The low-energy phonons dispersion along (1 1 1) is generally in agreement with theoretical calculations with two notable exceptions. First, the longitudinal-optical (LO) mode is hardened in experiments (the hardening is 7 meV at zone border). Furthermore, although the sound velocity of the longitudinal-acoustic mode is in good agreement with DFT calculations, above $q = 0.1$ and about 8 meV, the longitudinal-acoustic branch (LA) suddenly bends, and its energy at the zone boundary is 11.4 ± 0.1 meV, according to INS, which is very close to that of the calculated first transverse-optical mode at the zone boundary L (labeled TO in Fig. 4, top panel), at 11.8 meV. The same behavior can be observed on the high-energy section of the LA mode. Close to the zone boundary, from $q = 0.5$ to $q = 0.3$, the dispersion, as measured with both INS and IXS, reproduces very well the calculated one. Then it departs from the theoretical prediction going toward the zone center, below $q = 0.3$ and 16 meV. Finally toward zone center the LA mode flattens to a value of ≈ 10 meV, slightly lower than what observed at L. Note, that the calculated energy for the TO mode at zone center Γ is substantially higher, namely, 13.9 meV.

This behavior is reminiscent of an avoided crossing, or anticrossing, where the longitudinal-acoustic mode interacts
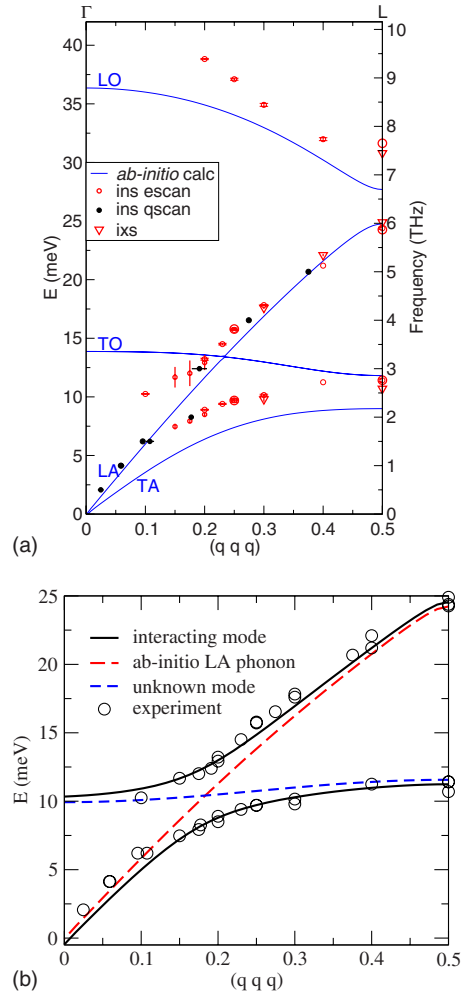

FIG. 4. (Color online) Top panel: phonon dispersion along the (1 1 1) direction. Hollow and filled circles indicate, respectively, constant Q and constant energy INS scan. Triangles represent IXS constant Q scan. Lines represents *ab initio* calculated phonon dispersion. The scans are of type $Q_z \times (1\ 1\ 1) + (q\ q\ q)$ with and $Q_z = 1, 2, 3$, in rhombohedral lattice. Using standard notation, we label LA and TA the longitudinal- and transverse-acoustic modes, respectively. We label LO and TO longitudinal- and transverse-optical modes, respectively. Bottom panel: zoom on the low-energy part of the above dispersion data. Circles indicate the experimental points (IXS and INS together). Dashed lines show the dispersion of the *ab initio* longitudinal-acoustic phonon and of the unknown mode. Continuous lines show the dispersion of the interacting mode described by Eq. (2), fitted to the experimental data.

with an unknown mode. To analyze the experimental data, we suppose that the dispersion of the unknown mode is described by

$$\epsilon(q) = a + b \cos(2\pi q), \qquad (1)$$

where a and b are fitting parameters and $(q\ q\ q)$, is the momentum in the rhombohedral coordinates. We consider a q-independent coupling Δ with the longitudinal-acoustic phonon. Within this model, the excitation energies, observed in the inelastic experiments, are the eigenvalues of a 2×2 matrix,
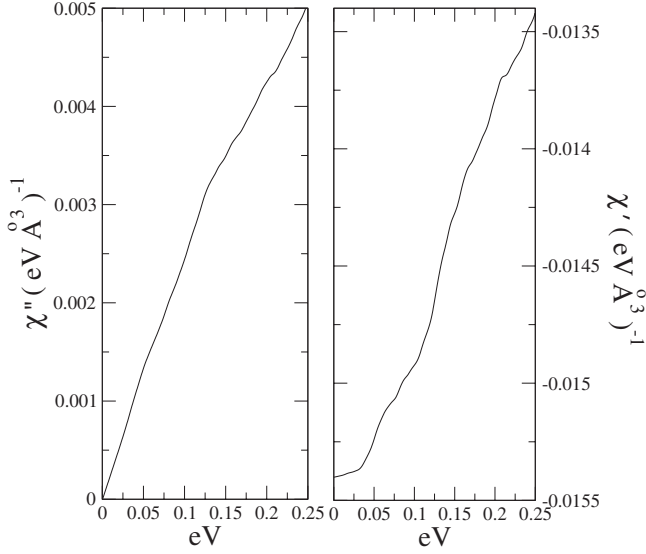
FIG. 5. Real and imaginary part of the susceptibility for CaC$_6$.

$$\begin{pmatrix} \epsilon(q) & \Delta \\ \Delta & \hbar\omega_{\mathrm{LA}}(q) \end{pmatrix}, \qquad (2)$$

where $\hbar\omega_{\mathrm{LA}}(q)$ is the longitudinal-acoustic phonon energy, as calculated using DFT. By minimizing the mean-square error between the computed and observed energies, we obtain a good fit with $a=10.75$ meV, $b=-0.82$ meV, and $\Delta=2.06$ meV, see Fig. 4 (bottom panel). As a consequence the detected anomaly can be explained by the coupling of the longitudinal-acoustic phonon mode with a longitudinal excitation or defect mode of unknown origin.

The first optical mode is transverse supposing $R\bar{3}m$ symmetry, and therefore silent in this configuration, as it can be seen in the simulated spectra in Fig. 3. An interpretation of the anticrossing could be that the aforementioned first optical mode would be activated by some symmetry-breaking scattering, as from impurities, which would mix different polarizations. However, the dispersion, flat within error bars, or even with a slight positive slope at zone center, is not compatible with the negative slope of the first optic.

A second possibility, could be the coupling to a longitudinal low-energy plasmon. Indeed in another layered material, MgB$_2$, an acoustic plasmon mode was indeed detected at surprisingly low energy.[23] To address this issue we calculate the **G**$=0$ and **G**$'=0$ bare susceptibility, namely,

$$\chi_{\mathbf{q}}(\omega) = \chi_{\mathbf{q}}(\mathbf{G}=\mathbf{0}, \mathbf{G}'=\mathbf{0}, \omega) = \frac{1}{N_{\mathbf{k}}\Omega}$$

$$\times \sum_{\mathbf{k}, nm} \frac{|\langle \psi_{\mathbf{k}n} | e^{-i\mathbf{q}\cdot\mathbf{r}} | \psi_{\mathbf{k}+\mathbf{q}n'} \rangle|^2 (f_{\mathbf{k}n} - f_{\mathbf{k}+\mathbf{q}m})}{\epsilon_{\mathbf{k}n} - \epsilon_{\mathbf{k}+\mathbf{q}m} + \omega - i\eta}, \quad (3)$$

where $\Omega=496.38\ a_0^3$ is the unit-cell volume with $a_0=\frac{\hbar^2}{me^2}=0.53$ Å the Bohr radius and $f_{\mathbf{k}n}$ is the Fermi function for a band energy $\epsilon_{\mathbf{k}n}$. Since the calculation of Eq. (3) requires a very accurate sampling of the Brillouin zone, we calculate the matrix element using first-principles calculations on a 6
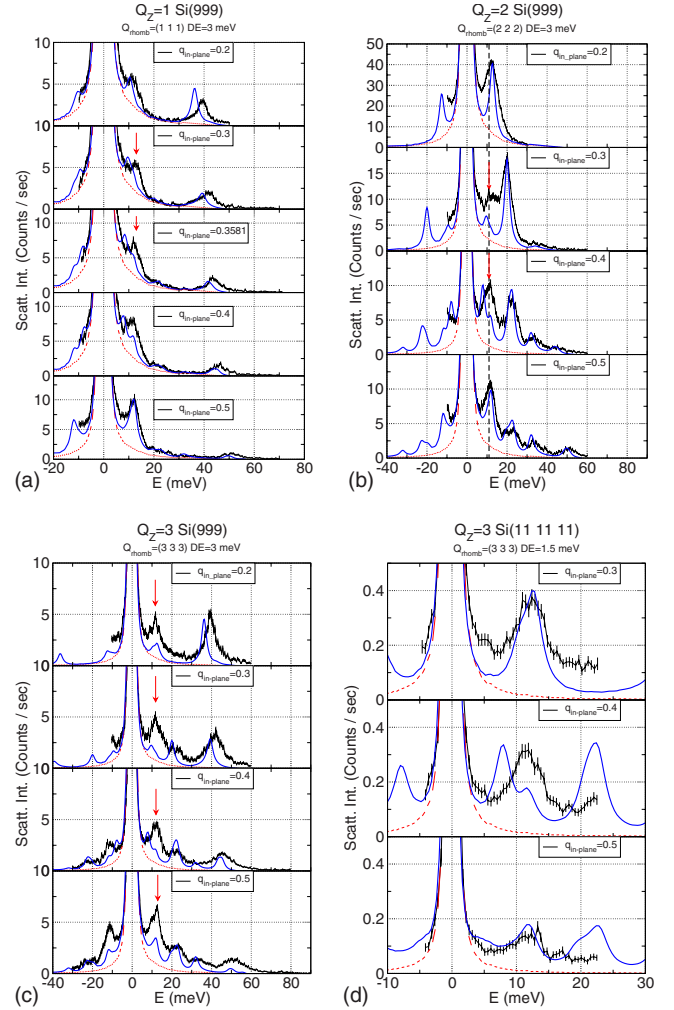

FIG. 6. (Color online) Constant-Q in-plane phonon density of states obtained using IXS (line with error bars) compared to *ab initio* calculations (thick lines). The experimental elastic contribution is also shown (thin lines). The scans are obtained at **G**+**q**, where **G**$=Q_z \times (111)$ and $Q_z=1$ (top, left), $z=2$ (top, right), $z=3$ (bottom), while **q** lies in plane and we give its modulus along the $(1\bar{1}0)$ direction in reduced length units for each spectra. For both top panels the energy resolution is 3 meV. For the bottom panels the energy resolution setup is 3 meV (left) and 1.5 meV (right). Calculations are normalized to the mode at about 50 meV in the left panel while normalization is to the lowest-energy mode in the right panel.

$\times 6 \times 6$ grid and then we interpolate it all over the Brillouin zone using Wannier interpolation.[24–26] In order to obtain a good description of the CaC$_6$ first-principles bands, we use seven Wannier functions. Then we interpolate the matrix element and the band structure over a $N_k = 150 \times 150 \times 300$ k-points grid and calculate $\chi_{\mathbf{q}}(\omega)$ at $q=(0.25, 0.25, 0.25)$, close to where the anticrossing occurs. The temperature in the Fermi function is $T=300$ K and the Lorentzian smearing $\eta=4$ meV. The results for the real (χ') and imaginary (χ'') part of the susceptibility are shown in Fig. 5.

A peak in the imaginary part of $\chi_{\mathbf{q}}(\omega)$ would signal the occurrence of a plasmon excitation. In our case the imaginary part of the susceptibility is featureless. Thus no plasmon excitations are present in CaC$_6$ calculated susceptibility. To

cross-check our result we also consider the case of MgB_2 where a plasmon was found.[23] In the MgB_2 case we reproduce the occurrence of an acoustic plasmon mode in agreement to Ref. [23]. As a consequence the 11 meV excitations is unlikely to be due to a longitudinal plasmon but most likely to impurities.

A possible origin of the impurity mode would be the presence of lithium in the preparation of the samples by liquid-solid synthesis method.[9] This hypothesis is supported by a strong x-ray photoemission spectroscopy signal for the lithium ion at the K edge (results not shown). However, this measurements are not confirmed by nuclear microprobe analysis.

A further possibility would be the presence of a $P6_3/mmc$ phase in the sample coexisting with the most stable $R\bar{3}m$ one. However the attempt to describe the c-axis phonon dispersion in terms of a similar $P6_3/mmc$ phase is also unsatisfactory since the dispersion of the low-energy modes is hardly distinguishable from the dispersion of the $R\bar{3}m$ phase. Still it is possible that the avoided crossing is generated by the presence of vacancies or other similar defects.

An anomaly at a similar energy is also observed in another set of data which consists in constant-Q two-dimensional phonon density of states with a propagation vector **q** lying in the plane perpendicular to the (1 1 1) direction and corresponding to the a^*b^* plane. For this IXS experiment, the choice of $\mathbf{G}=Q_z\times(1,1,1)$, with $Q_z\neq0$ resulted in a significant contribution from transverse modes. In this respect what is measured is a two-dimensional density of states obtained averaging over all the structure factors having modulus of the IXS exchanged momentum $|\mathbf{G}+\mathbf{q}|$, where $|\mathbf{q}|$ is in the plane as reported in Figs. 2 and 6. Even if the measurement is not equivalent to a phonon-dispersion calculation, as both longitudinal and transverse modes are measured, the low-energy modes are fairly well reproduced, except for an extra intensity measured at about 10–13 meV for all Q_z, in particular, for the spectra with q from 0.3 to 0.4, (see arrows in Fig. 6) in agreement to what we found along the c axis.

In a recent paper on a comparable sample of CaC_6,[8] using IXS only, Upton *et al.* incorrectly assigned the flat band at $\sim$11 meV to the first transverse-optical mode. This is due to the fact that they lack both a symmetry analysis of their calculated modes as well as the resolution necessary to see

the details of the anticrossing. Note that the region close to zone center, below $q=0.15$, is difficult to measure using IXS due to the large elastic peak at zero energy generated by disorder. This is not the case in INS scattering data and only by using this experimental technique the avoided crossing behavior between the LA mode and an unknown mode can be revealed.

We note that, using the in-plane configuration with IXS, we found good agreement between the data and the simulation in the 50 meV energy region. This is particularly important as vibrations propagating in-plane in this energy window are supposed to be among the ones contributing to electron-phonon mechanism.[4,27]

IV. CONCLUSIONS

In conclusion, we show that low-energy phonon structure of the superconducting graphite intercalated compound CaC_6, show clear anomalies, in disagreement with DFT calculations assuming the perfect-crystal structure. In particular, we observe an anticrossing of the acoustic longitudinal mode with an additional longitudinal flat mode. Calculation of the electron susceptibility suggests that this mode cannot be attributed to a plasmon excitation. Thus we infer that the unknown excitation is most likely due to defects, impurities, or vacancies. On the other hand, we found good overall agreement between the data and the simulations, particularly in the 50 meV energy region where the C_z vibrations propagating in plane in this energy window are supposed to provide the largest contribution to electron-phonon mechanism.

---

*matteo.dastuto@impmc.upmc.fr

†Present address: Laboratoire de Spectrometrie Physique, Université Joseph Fourier, 140 Av. de la physique, BP 87-38402, Saint Martin d'Hères, France.

‡Institut de Minéralogie et de Physique des Milieux Condensés (IMPMC), CNRS UMR 7590, Campus Boucicaut, 140 rue de Lourmel, 75015 Paris, France.

§Present address: University of Aberdeen, Chemistry Department, Meston Walk, Aberdeen AB24 3UE, Scotland.

‖Present address: Diamond Light Source, Diamond House, Harwell Science and Innovation Campus, Didcot, Oxfordshire OX11 0DE, England.

[1] T. Enoki, M. Suzuki, and M. Endo, *Graphite Intercalation Compounds and Applications* (Oxford University Press, Oxford, New York, 2003).

[2] E. Weller, M. Ellerby, S. S. Saxena, R. P. Smith, and N. T. Skipper, Nat. Phys. **1**, 39 (2005).

[3] N. Emery, C. Hérold, M. d'Astuto, V. Garcia, C. Bellin, J. F. Marêché, P. Lagrange, and G. Loupias, Phys. Rev. Lett. **95**, 087003 (2005).

[4] M. Calandra and F. Mauri, Phys. Rev. Lett. **95**, 237002 (2005).

[5] J. S. Kim, L. Boeri, R. K. Kremer, and F. S. Razavi, Phys. Rev. B **74**, 214513 (2006).

[6] A. Sanna, G. Profeta, A. Floris, A. Marini, E. K. U. Gross, and S. Massidda, Phys. Rev. B **75**, 020511(R) (2007).

[7] I. I. Mazin, L. Boeri, O. Dolgov, A. Golubov, G. Bachelet, M. Giantomassi, and O. K. Andersen, Proceedings of the M2S Conference, Dresden, 2006 (unpublished).

[8] M. H. Upton, A. C. Walters, C. A. Howard, K. C. Rahnejat, M. Ellerby, J. P. Hill, D. F. McMorrow, A. Alatas, B. M. Leu, and W. Ku, Phys. Rev. B **76**, 220501(R) (2007).

[9] S. Pruvost, C. Hérold, A. Hérold, and P. Lagrange, Eur. J. Inorg. Chem. **2004** (8), 1661 (2004).

[10] See supplementary material at http://link.aps.org/supplemental/ 10.1103/PhysRevB.81.104519 for the magnetization density measurements of the sample used in the present work.

[11] E. Burkel, *Inelastic Scattering of X-rays with Very High Energy Resolution*, Springer Tracts in Modern Physics Vol. 125 (Springer, Berlin, 1991).

[12] J. Maultzsch, S. Reich, C. Thomsen, H. Requardt, and P. Ordejón, Phys. Rev. Lett. **92**, 075501 (2004).

[13] N. Emery, C. Hérold, and P. Lagrange, J. Solid State Chem. **178**, 2947 (2005).

[14] R. Verbeni *et al.*, J. Synchrotron Radiat. **3**, 62 (1996).

[15] R. Verbeni, M. d'Astuto, M. Krisch, M. Lorenzen, A. Mermet, G. Monaco, H. Requardt, and F. Sette, Rev. Sci. Instrum. **79**, 083902 (2008).

[16] C. Masciovecchio, U. Bergmann, M. Krisch, G. Ruocco, F. Sette, and R. Verbeni, Nucl. Instrum. Methods Phys. Res. B **111**, 181 (1996).

[17] M. d'Astuto, M. Calandra, S. Reich, A. Shukla, M. Lazzeri, F. Mauri, J. Karpinski, N. D. Zhigadlo, A. Bossak, and M. Krisch, Phys. Rev. B **75**, 174508 (2007).

[18] P. Giannozzi *et al.*, J. Phys.: Condens. Matter **21**, 395502 (2009).

[19] S. Baroni, S. de Gironcoli, A. Dal Corso, and P. Giannozzi, Rev. Mod. Phys. **73**, 515 (2001).

[20] J. P. Perdew, K. Burke, and M. Ernzerhof, Phys. Rev. Lett. **77**, 3865 (1996).

[21] D. Vanderbilt, Phys. Rev. B **41**, 7892 (1990).

[22] M. Calandra and F. Mauri, Phys. Rev. B **74**, 094507 (2006).

[23] V. M. Silkin, A. Balassis, P. M. Echenique, and E. V. Chulkov, Phys. Rev. B **80**, 054521 (2009).

[24] A. A. Mostofi, J. R. Yates, Y.-S. Lee, I. Souza, D. Vanderbilt, and N. Marzari, Comput. Phys. Commun. **178**, 685 (2008).

[25] I. Souza, N. Marzari, and D. Vanderbilt, Phys. Rev. B **65**, 035109 (2001).

[26] N. Marzari and D. Vanderbilt, Phys. Rev. B **56**, 12847 (1997).

[27] K. Sugawara, T. Sato, and T. Takahashi, Nat. Phys. **5**, 40 (2009).